POLYOXOMETALATES

Open Access
RESEARCH ARTICLE

Facile construction of polyoxometalate-modified polyaryletherketone-based hybrid membranes with enhanced proton conductivity

Bo Hu[1,§], Qiuchen Du[2,§], Yang Yang[2], Dengdeng Li[2], Jiawang Fu[2], Bailing Liu[2,3] ✉, Hong-Ying Zang[1] ✉, Yangguang Li[1] ✉, Haiming Xie[1], and Zhongmin Su[4]

[1] *Department of Chemistry, Northeast Normal University, Changchun 130024, China*
[2] *Department of Chemistry and Environmental Engineering, Changchun University of Science and Technology, Changchun 130022, China*
[3] *Chongqing Research Institute, Changchun University of Science and Technology, Chongqing 401120, China*
[4] *State Key Laboratory of Supramolecular Structure and Materials, Institute of Theoretical Chemistry, College of Chemistry, Jilin University, Changchun 130021, China*
[§] *Bo Hu and Qiuchen Du contributed equally to this work.*

Cite This: *Polyoxometalates*, **2025**, *4*, 9140079

Read Online

ABSTRACT: The development of novel proton exchange membranes (PEMs) with high proton conductivity and good mechanical performance as alternatives to Nafion is crucial. Polyoxometalates (POMs), a type of solid-state nanoclusters, possess high proton conductivity and good structural stability, making them suitable functional inorganic fillers to improve the performance of PEMs. Herein, the Keggin-type POM $H_3PW_{12}O_{40}{\cdot}nH_2O$ (PW_{12}) was introduced into sulfonated polyaryletherketone (SPAEK) with closely packed and flexible side chains to construct hybrid membranes (SPAEK-PW_{12}-*x*%, *x* = 5, 10, 13, 15). Because of its structural characteristics, the nanosized PW_{12} induced precise hybridization of the nanophase structure of this ionomeric polymer and the formation of proton transport channels. Additionally, the hydrogen-bonding networks formed by PW_{12} and sulfonic acid groups increased the proton conductivity and mechanical strength of the resulting hybrid PEMs and improved the close-packed structure of the PEMs to achieve an appropriate balance between conductivity and fuel permeation. In particular, SPAEK-PW_{12}-13% achieved an enhanced proton conductivity of 0.167 S·cm^{-1} at 80 °C, which was 2.2 times greater than that of the pristine membrane. Moreover, the mechanical properties, chemical stability, resistance to methanol penetration, and ionic selectivity of the hybrid membrane were significantly improved upon addition of a moderate amount of PW_{12}. This work provides an approach for the design and development of new-generation organic–inorganic hybrid membranes through precise hybridization of POMs.

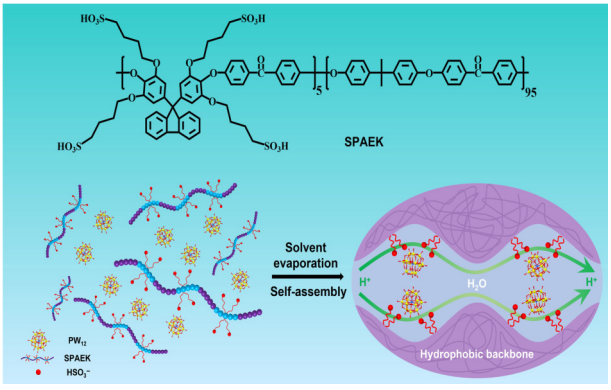

KEYWORDS: polyoxometalates, sulfonated polyaryletherketone, proton exchange membrane, proton conduction

1 Introduction

Proton exchange membrane fuel cells (PEMFCs) are among the most important renewable energy conversion devices and have attracted a considerable amount of attention because of their high energy density and environmental friendliness [1–4]. As a crucial component of PEMFCs, proton exchange membranes (PEMs) play irreplaceable roles in proton conduction and fuel blocking to achieve high proton conductivity and structural stability [5, 6]. Because of their excellent proton conductivity and outstanding electrochemical stability, perfluorosulfonic acid polymers, such as commercial Nafion, which have a distinct phase-separated morphology and continuous long-range proton transport channels, are widely used in PEMFCs [7, 8]. Nevertheless, the high costs, complex fabrication processes, severe fuel permeation, and performance degradation in high-temperature environments restrict the application of these polymers [9]. Thus, it is necessary to find alternatives to improve the performance of fuel cells.

Because of their designable structure, acceptable mechanical qualities, and low manufacturing costs, various aromatic hydrocarbon polymers containing proton exchange groups, such as sulfonated polyarylethers (SPAEs), sulfonated poly(aryl ether ketone)s (SPAEKs), sulfonated polyimides (SPIs), and sulfonated

Received: July 30, 2024; **Revised:** August 31, 2024
Accepted: September 11, 2024

✉Address correspondence to Bailing Liu, liubl@cust.edu.cn; Hong-Ying Zang, zanghy100@nenu.edu.cn; Yangguang Li, liyg658@nenu.edu.cn

polysulfone's (SPSUs), have been used to develop PEMs to identify a suitable material to replace Nafion [10]. However, the proton exchange groups in the abovementioned polymers are directly connected to their main chains with a random distribution, resulting in unavoidable dead ends in the proton transport channels of the developed PEMs. Although some technical strategies can improve the degree of sulfonation of the polymer and increase the continuity of the proton transport channel, such strategies also lead to excessive expansion of the PEM and poor mechanical properties. Compared to strategies that directly increase the ion exchange capacity (IEC) of the membrane, strategies that optimize the proton channels in the PEMs and improve the proton conduction efficiency can better improve the comprehensive performance of PEMs. Thus, various functionalized nanofillers [11–19], such as metal organic frameworks (MOFs) [20], zirconium dioxide nanotubes (ZrNTs) [21], graphene [22], and carbon nanotubes (CNs) [23], have been incorporated to improve the water retention capacity and proton conductivity of PEMs. Despite these advancements, a need remains to design and develop new organic–inorganic hybrid membrane to achieve efficient proton transport.

Polyoxometalates (POMs), which are metal–oxygen clusters composed of high-valence transition metals, have often been used as proton conductors and functional inorganic fillers in PEMs [24–31]. Compared to the common large inorganic fillers, POMs have remarkable advantages owing to their nanoscale size, high proton conductivity, good stability, and strong redox activity [31–39]. Because of their composition and structural characteristics, POMs may act as proton sources and dissolve to form polyoxoanions and hydrated protons (such as H^+, H_3O^+, and H_5O^{2+}) in humid environments. Additionally, abundant oxygen atoms on the surface of polyoxoanions can serve as hopping sites for protons, providing ample carriers for the construction of hydrogen-bonding networks [40, 41]. The delocalization of negative charges on the surfaces of nanosized polyanions endows POMs with a low negative charge density that facilitates the dissociation and flow of protons [42]. For example, Su et al. synthesized a Ce-mediated molecularly tailorable product $\{Ce_{11}Mo_{96}\}$ based on an extremely large polymolybdate $\{Mo_{132}\}$ cluster, and it exhibited a high proton conductivity of 9.01×10^{-2} S·cm^{-1} at 80 °C and 98% relative humidity (RH) [43]. However, natural POM materials suffer from poor mechanical processing, which seriously limits their practical application in fuel cells [33]. Thus, hybrid materials prepared by blending POMs with a polymer matrix have significant advantages for use as substitutes for POM bulk materials. Liu et al. synthesized hydrogel composites composed of a POM-based inorganic–organic hybrid, poly(vinyl alcohol) (PVA), and glycerol (Gly), and these composites exhibited a proton conductivity of 1.11×10^{-2} S·cm^{-1} at ambient humidity and 75 °C and good mechanical properties [44]. As inorganic fillers, POMs are comparable in size to the nanophases of PEMs so that can be used to modify membranes without disturbing their continuous phase morphology. On the basis of the above-described theory, our group fabricated a series of high-performance hybrid PEMs by incorporating nanoscale bismuth oxide clusters into Nafion, and these PEMs exhibited high proton conductivity, low methanol permeability, and ideal mechanical and chemical stabilities [45]. Li's group introduced a polyethylene glycol-grafted POM amphiphile ($GSiW_{11}$) into Nafion to prepare a series of hybrid membranes that exhibited the highest proton conductivity of 226 mS·cm^{-1} at 80 °C and a 130% enhancement in power density [46]. Recently, Lan et al. prepared hybrid PEMs by introducing 2MeIm-$\{Mo_{132}\}$ into SPAEKs, and these PEMs exhibited an enhanced proton conductivity of 75 mS·cm^{-1} and a maximum power density of 266.2 mW·cm^{-2} at 80 °C [47]. All these results demonstrate that POMs can be used as nanofillers to modify PEMs based on aromatic hydrocarbon polymers containing pendant sulfonic acid groups by the formation of a three-dimensional (3D) proton transfer pathway in the POM-containing hybrid composite PEMs.

Inspired by the abovementioned studies, we attempted to introduce $H_3PW_{12}O_{40}{\cdot}nH_2O$ (PW_{12}) into SPAEKs with a high density of flexible side chains to construct hybrid membranes. In our strategy, the introduction of flexible side chains into SPAEKs was expected to contribute to phase separation, resulting in an improvement in the proton conductivity of the resulting PEMs without increasing the degree of sulfonation of the polymer matrix. Because of its structural characteristics, nanosized PW_{12} can freely enter the hydrophilic phase of membranes and participate in the formation of proton transport channels. Furthermore, hydrogen-bonding networks formed by PW_{12} and sulfonic groups can increase the proton conductivity of the hybrid membrane and improve the close-packed structure of PEMs to achieve an appropriate balance between conductivity and fuel permeation. As a result, the proton conductivity of the hybrid membranes prepared in this study reached up to 0.167 S·cm^{-1} at 80 °C (SPAEK-PW_{12}-13%), which was 2.2 times greater than that of pristine membrane, and the methanol permeability of the membranes simultaneously decreased by an order of magnitude. Thus, this study describes a concept based on nanosized hybridization for the construction of advanced PEMs.

2 Experimental

2.1 Materials

2,6-Dimethoxyphenol, 9-fluorenone, and mercaptopropionic acid (MPA) were purchased from Aladdin Reagent Co. (Shanghai). 4,4'-Difluorobenzophenone (DFBP), bisphenol A (BPA), boron tribromide (BBr_3), and 1,4-butanesultone were purchased from Macklin. Dimethylacetamide (DMAc), dimethyl sulfoxide (DMSO), dichloromethane, and other solvents and reagents (AR grade) were purchased from Sinopharm Chemical Reagent Company and used as received. Toluene, DMAc, DMSO, and dichloromethane were used after dehydration.

2.2 Synthesis of 9,9-bis(3,5-dimethoxy-4-hydroxyphenyl) fluorene (DMHF)

DMHF was synthesized from 2,6-dimethoxyphenol and 9-fluorenone in accordance with previous literature [48] (Figs. S1 and S2 in the Electronic Supplementary Material (ESM)). A light yellow crude product was recrystallized three times in toluene to obtain a pure white solid product in 92.9% yield. ^{1}H nuclear magnetic resonance (NMR) (δ, 500 MHz, DMSO-d_6): 8.34 (s, 2H, –OH), 3.53 (s, 12H, $-OCH_3$), 7.90 (d, 2H, H_a), 7.39 (t, 2H, H_b), 7.31 (t, 2H, H_c), 7.51 (d, 2H, H_d), 6.32 (s, 4H, H_e).

2.3 Synthesis of methoxy-functionalized poly(aryl ether ketone) (MPAEK)

As shown in Scheme 1, MPAEK copolymers were synthesized from DMHF, DFBP, and BPA. A typical synthesis was performed as

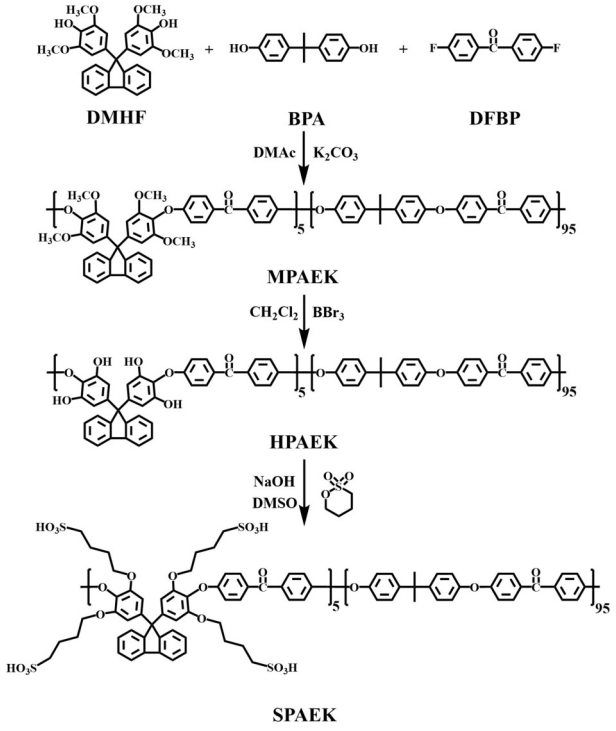

Scheme 1 Synthesis of polymers MPAEK, HPAEK and SPAEK.

follows: First, 1.6938 g (3.6 mmol) of DMHF, 7.3966 g (32.4 mmol) of BPA, 7.8552 g (36 mmol) of DFBP, and 7.482 g (54 mmol) of K_2CO_3 were dissolved in a mixture of 126 mL of DMAc and 72 mL of toluene under a nitrogen atmosphere. The resulting mixture was heated to 140 °C and refluxed for 8 h. Then, the temperature was increased to 165 °C and maintained for 12 h. After cooling, the obtained viscous solution was diluted with 40 mL of DMAc and then poured into methanol to obtain precipitated polymers. These polymers were then filtered and washed three times. The final products (named MPAEK) were collected after vacuum drying at 120 °C for 24 h.

2.4 Synthesis of hydroxylated poly(aryl ether ketone) (HPAEK)

Demethylation was performed as follows. A mixture of MPAEK (3.00 g) and anhydrous dichloromethane (150 mL) was introduced into a three-necked round-bottom flask equipped with a nitrogen inlet. The mixture in the flask was purged with dry nitrogen for 1 h in an ice bath. Then, BBr_3 (1.8 mL) was slowly added, and the solution gradually darkened as blood-red solids formed. After 6 h, the solid products were filtered and washed several times with CH_2Cl_2. The solids were then transferred into deionized water and washed by refluxing for 48 h. After the color of the solids disappeared, the resulting products (named HPAEK) were collected by vacuum drying at 100 °C for 24 h (89% yield).

2.5 Synthesis of sulfonated poly(aryl ether ketone) (SPAEK)

Sulfonation was performed as follows. HPAEK (4.0 g) was dissolved into 80 mL of DMSO at room temperature with stirring for 1 h under a nitrogen atmosphere. Then, 0.496 g of NaOH and 1,4-butanesultone (1.69 mL) were added to the above solution, and the temperature was increased to 110 °C for 12 h. The resulting transparent solution was slowly poured into a large amount of isopropyl alcohol, and white flocculent solids formed. After being filtered and washed repeatedly with deionized water, the final product (named SPAEK) was collected and dried at 100 °C under vacuum for 24 h (92% yield).

2.6 Preparation of hybrid membranes

SPAEK-PW_{12}-x% hybrid membranes were prepared by means of the solution-casting method. The preparation of the SPAEK-PW_{12}-13% hybrid membrane was provided as an example: First, 0.3 g of dried SPAEK, 0.039 g of $H_3PW_{12}O_{40}{\cdot}nH_2O$, and 2.98 mL of DMSO were dissolved and vigorously stirred for 10 h at ambient temperature to form a homogeneous solution. The solution was cast onto a glass plate and dried at 80 °C for 12 h to obtain a membrane. To acidify the membrane, the film was peeled off the glass plate and immersed into 2 M H_2SO_4 for 24 h. Afterward, the acidified membrane was washed repeatedly with deionized water to neutral pH and then stored in deionized water until needed for testing. A series of hybrid membranes, SPAEK-PW_{12}-x%, were prepared according to the above synthesis scheme. The hybrid membranes were named SPAEK-PW_{12}-x%, where x = 0, 5, 10, 13, 15 is the weight percentage of the filler (PW_{12}) in SPAEK. The thicknesses of all the obtained membranes were 40–100 μm.

3 Results and discussion

3.1 Synthesis and characterization of the copolymers and hybrid membranes

As illustrated in Scheme 1, a matrix of membranes was synthesized through copolymerization of DMHF, DFBP, and BPA before further modifications. To maintain the proton conductivity and mechanical properties of the pristine SPAEK membrane, the molar proportion of DMHF units in the copolymers, which ultimately determined the degree of sulfonation of the membranes, was set as 5%. The chemical structures of the synthesized copolymers were characterized by ^{1}H NMR spectroscopy (Fig. S3 in the ESM). In the spectrum of MPAEK, the peaks at 3.5 and 1.65 ppm were attributed to methoxy groups in the DMHF unit and H_j atoms in the bisphenol A unit, respectively. The peaks from 6.4 to 8 ppm were attributed to aromatic protons in the backbone of the copolymers. These data confirmed the synthesis of MPAEK with a molecular weight of ~ 37,210 in 92% yield. The methoxy groups were converted into hydroxyl groups in CH_2Cl_2 using BBr_3, and the products were precipitated and collected in 89% yield. In the spectra of HPAEK, the methoxy peak at 3.5 ppm disappeared, and a new peak appeared at 9.4 ppm that was attributed to the protons in the hydroxyl groups. This result indicated the successful preparation of HPAEK. HPAEK was then sulfopropylated via nucleophilic ring-opening to generate sulfonated copolymers of SPAEK in 92% yield. After this reaction, the peak at 9.43 ppm, which was attributed to –OH, disappeared completely, and new peaks appeared at 2.33, 3.78, 1.67, and 1.47 ppm, which were attributed to the butanesulfonic methylene protons (H_n, H_k, H_l, and H_m). Notably, the peak attributed to H_e changed from a sharp single peak to multiple lower-intensity peaks because the steric hindrance of the large butane sulfonate groups prevented free rotation of the benzene ring, which further proved the successful synthesis of the polymer SPAEK.

SPAEK-PW_{12}-x% hybrid membranes with different amounts of

PW_{12} were prepared via a solution-casting technique, in which PW_{12} clusters were hybridized into the ionic nanophase of SPAEK membranes through intermolecular polar interactions and hydrogen-bonding interactions (Scheme 2). The hydrophilic nanostructure of the SPAEK membranes was sensitive to additives and the self-assembly environment. Therefore, our precise molecular-level targeted assembly strategy could be effectively used to fabricate hybrid SPAEK membranes with desired nanoscale architectures. To illustrate this precise selected targeted assembly strategy, various characterization techniques were used to analyze the chemical composition, self-assembly mechanism, and physical–chemical properties of the prepared hybrid membranes.

Fourier transform infrared (FTIR) spectra of SPAEK-PW_{12}-x% (x = 0, 5, 10, 13, 15) are shown in Fig. 1(a). The broad absorption band at approximately 3400 cm^{-1} was ascribed to the stretching vibration of O–H. The peak at ~ 2960 cm^{-1} was attributed to aromatic –CH stretching. The peak at 1036 cm^{-1} was attributed to symmetric stretching vibrations of phenyl ether bonds. The peaks at 1305 and 1490 cm^{-1} were attributed to asymmetric stretch vibrations of phenyl ether bonds. The distinctive signals at 1009 and 1140 cm^{-1} arose from the stretching vibrations of S–O and S=O, respectively. In the spectrum of PW_{12}, four absorption peaks were observed at 1080, 986, 897, and 802 cm^{-1}, which were attributed to the stretching vibrations of P–O_c, W=O_t, W–O_b–W, and W–O_e–W, respectively (O_c, O_t, O_b, and O_e represent the central oxygen, terminal oxygen, bridged oxygen of two octahedra sharing a corner, and bridged oxygen of two octahedra sharing an edge, respectively) [49]. These four peaks were all enhanced as the amount of PW_{12} increased, as shown in Fig. 1(a).

Thermogravimetric analysis (TGA) was employed to study the thermal stability of the membranes (Fig. S4 in the ESM). All the membranes exhibited three stages of weight loss over the entire temperature range (30–800 °C). The first stage of weight loss occurred before 200 °C and was attributed to the evaporation of the residual solvent and adsorbed water in the hybrid membrane. Notably, the weight loss of the hybrid membranes was greater than that of the pristine membrane during this stage. The main reason for this difference was that the hydrophilic molecules of PW_{12} could adsorb more crystal water, thus improving the weight loss of the hybrid membrane. The second weight loss stage, which occurred at approximately 200–350 °C, was attributed to degradation of the sulfonic acid group on the side chain. During this stage, weight loss of the hybrid membrane was significantly slower than that of the pristine membrane because PW_{12} was able to form strong hydrogen bonds with the sulfonic acid groups on the side chains of SPAEK. This interaction effectively improved the thermal stability of the side chains containing sulfonic acid groups and thus increased the decomposition temperature of the hybrid membrane. The third weight loss stage occurred at 370–800 °C and was attributed to degradation of the main chains of the polyaryl ether ketone

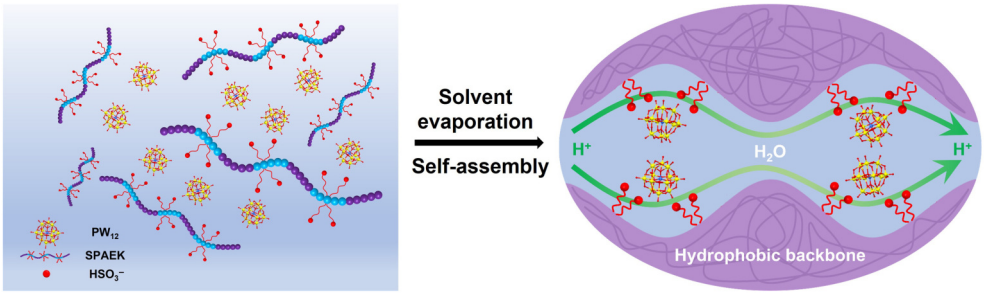

Scheme 2 Schematic of the proton conduction mechanism of SPAEK-PW_{12}.

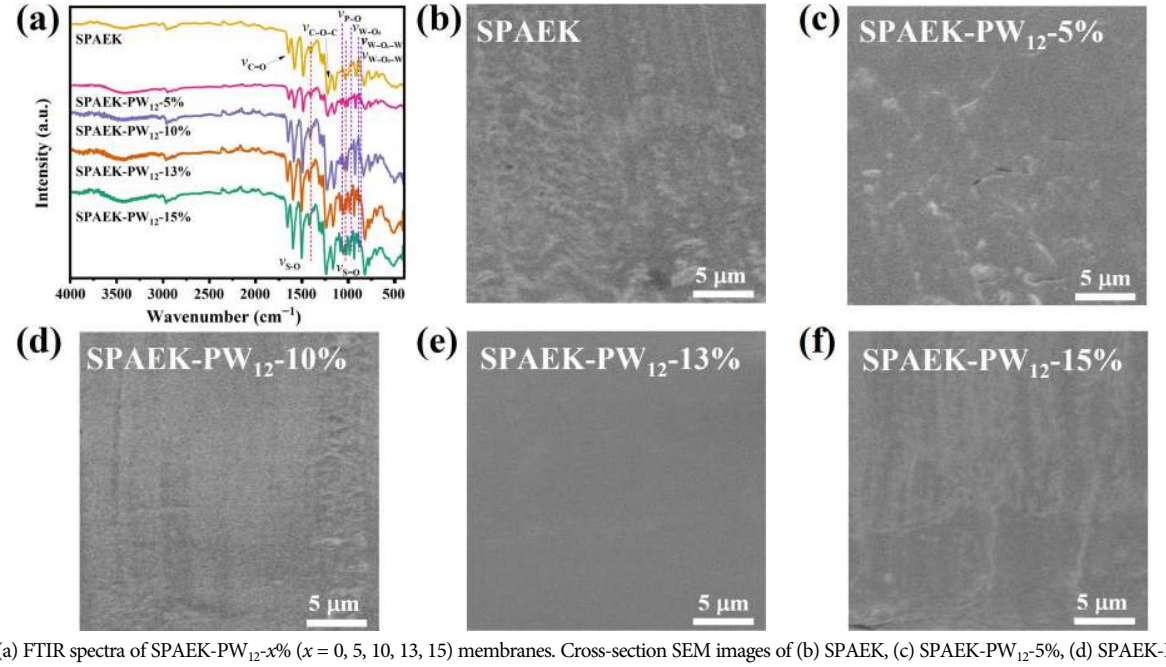

Figure 1 (a) FTIR spectra of SPAEK-PW_{12}-x% (x = 0, 5, 10, 13, 15) membranes. Cross-section SEM images of (b) SPAEK, (c) SPAEK-PW_{12}-5%, (d) SPAEK-PW_{12}-10%, (e) SPAEK-PW_{12}-13%, and (f) SPAEK-PW_{12}-15% membranes.

backbone. The above results indicated that the hybrid membranes exhibited excellent thermal stability, satisfying the requirements for application in PEMFCs.

3.2 Morphology of membranes

The micromorphology of cross sections of the pristine and hybrid membranes were investigated by scanning electron microscopy (SEM) (Figs. 1(b)–1(f)). A rough surface with obvious defects was observed for the pristine membrane, indicating that the accumulation of polymer chains in the membrane was not sufficiently dense. With the addition of PW_{12}, the defect degree of the membrane decreased, and the smoothness of the hybrid membrane increased because of the formation of strong hydrogen-bonding interactions between the oxygen-containing moieties of PW_{12} and the sulfonic acid groups, resulting in a more compact structure of the polymer chains. However, the introduction of excess PW_{12} disrupted the close-packed structure within the hybrid membrane, resulting in an irregular membrane surface (Fig. 1(f)).

The nanoscale morphologies of the pristine and hybrid membranes were evaluated by transmission electron microscopy (TEM) (Figs. 2(a)–2(c)). All the membrane samples were immersed in a 1 M $AgNO_3$ solution to examine the internal morphology of the membranes. The dark areas represent hydrophilic regions that reacted with a dye, while the bright areas indicate hydrophobic regions within the membrane [50]. As seen by comparing the images of SPAEK and SPAEK-PW_{12}-13%, the wormlike continuous hydrophilic channels corresponding to the dark areas became more concentrated and elongated after addition of the hydrophilic PW_{12}. Compared to the pristine membrane, the hybrid membrane exhibited a more significant microphase separation structure, and the ionic transport channels became more organized. For the SPAEK-PW_{12}-15% membrane, the disruption of the hydrophilic channel continuity was attributed to the aggregation of excessive POMs.

The distribution of elements in the membranes was investigated via energy-dispersive X-ray spectroscopy (EDS, Figs. 2(d)–2(g), and Fig. S5 and Fig. S6 in the ESM). For SPAEK, S and O were evenly distributed throughout the membrane, demonstrating that the obtained membrane was uniform. After addition of PW_{12}, the distribution of W was similar to that of S, showing that the PW_{12} clusters were attracted to the hydrophilic sulfonic acid groups (Figs. 2(d) and 2(g)). Moreover, the PW_{12} clusters were uniformly distributed in the membrane without large-scale aggregation, as seen in the results for SPAEK-PW_{12}-15% (Fig. S6 in the ESM). Wide-angle X-ray diffraction patterns were then used to determine the distribution and crystallinity of SPAEK and SPAEK-PW_{12}-x% nanophase membranes (Fig. S7 in the ESM and Table 1).

Small-angle X-ray scattering (SAXS) was utilized to analyze the impact of the addition of PW_{12} on the microstructure of the resulting hybrid membranes. Figure 2(h) shows that two characteristic peaks were observed in the spectra of all of the samples. The peak at q = 0.16 nm^{-1} was attributed to crystallization of the main chains of SPAEK. The peak at approximately q = 0.2–0.3 nm^{-1} was attributed to the nanophase separation of the membranes. This occurred mainly because of the dense aggregation of flexible sulfonic acid groups on the side chains of SPAEK, resulting in the formation of a good phase separation structure within the membrane. As the incorporation of PW_{12} increased, the peaks attributed to ion clusters shifted toward regions with high q values, which increased from 0.22 to 0.29 nm^{-1}. According to d =

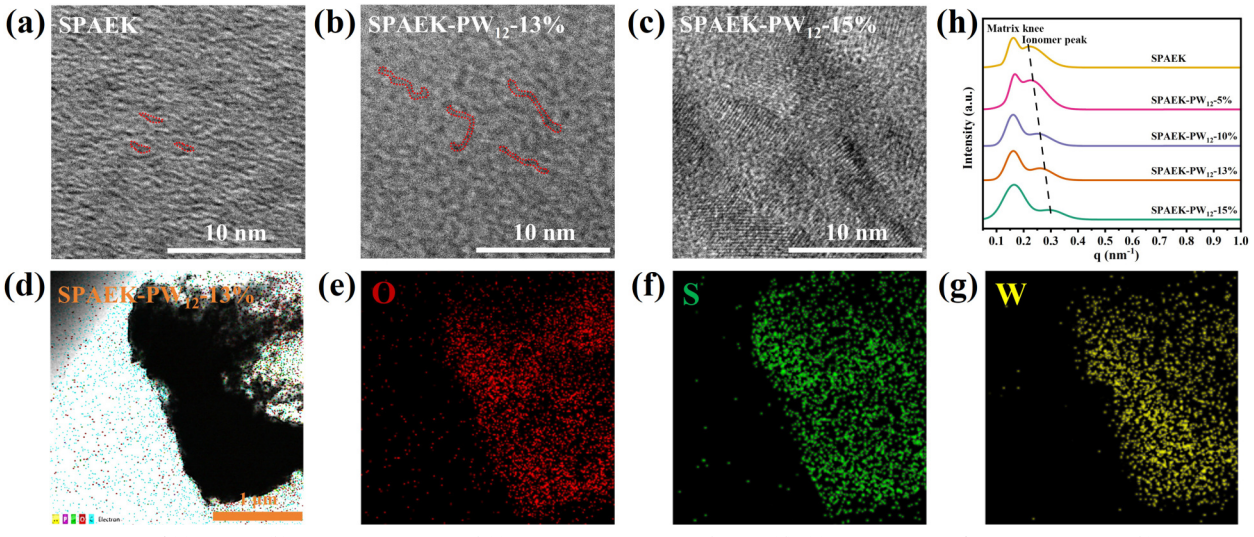

Figure 2 TEM images of (a) SPAEK, (b) SPAEK-PW_{12}-13% and (c) SPAEK-PW_{12}-15% membranes. (d)–(g) EDS mapping of SPAEK-PW_{12}-13%. (h) SAXS patterns of SPAEK-PW_{12}-x% (x = 0, 5, 10, 13, 15) membranes.

Table 1 Water uptake (WU), swelling ratio (SR), IEC, hydration number (λ) and crystallinity of membranes

Samples	WU (%) 80 °C	SR (%) 80 °C	IEC ($mmol \cdot g^{-1}$)	λ 80 °C	Crystallinity (%)
SPAEK	25.1	13.4	1.06	12.9	77.28
SPAEK-PW_{12}-5%	27.2	15.2	1.14	13.3	60.33
SPAEK-PW_{12}-10%	30.6	16.7	1.21	14.1	53.85
SPAEK-PW_{12}-13%	33.2	18.3	1.24	14.8	49.61
SPAEK-PW_{12}-15%	39.0	21.8	1.33	16.3	61.97

$2\pi/q$, the interval between the ionic phases in the hybrid membrane, defined by d, continued to decrease after incorporation of PW_{12} [51]. This occurred primarily because the PW_{12} molecules pulled the sulfonic acid groups in the hydrophilic phase closer together, ultimately leading to a denser distribution of ionic phases. These results are consistent with the trends observed in the TEM images. Noticeably, the crystallization peaks of the main chains associated with SPAEK-PW_{12}-15% became broader, mainly because of the large clusters that formed when excess PW_{12} accumulated and disrupted the regular alignment of the segments of the polymer chain, resulting in nonuniform crystallization of the polymeric main chains.

3.3 IEC, water uptake (WU), swelling ratio (SR), and hydration constant (λ) of the prepared membranes

As an important parameter for the evaluation of membranes, the IEC is closely related to other properties of PEMs, such as their WU and proton conductivity. The IEC values of the pristine and hybrid membranes were measured, and the results are displayed in Table 1. Because more protons dissociated from PW_{12} as the content increased, the IEC values of the membranes increased from 1.06 to 1.33 mmol·g^{-1}. Followed by the increased IEC values, the hybrid membrane exhibited higher values of WU, thus improving the proton conductivity of the membrane (Table 1 and Figs. 3(a) and 3(b)). Because of the unique side-chain architecture of SPAEK, a phase separation structure formed with hydrophobic and hydrophilic domains, thus enhancing the structural stability of the resulting PEMs. Figure 3(b) shows that the SR of the hybrid membranes increased as a result of the increased WU without excessive swelling. These results verify that the precise structural design of the polymer matrix played a significant role in improving the overall performance of the PEMs.

The λ value of the hybrid membrane represents the number of water molecules absorbed by each hydrophilic group. The experimental λ values of the hybrid membranes increased as the amount of PW_{12} increased. This parameter is an important indicator for assessing the hydration and proton conductivity of PEMs and directly impacts the ionic transmission mechanism of PEMs [52–54]. A high number of water molecules increase the concentration of water molecules in the membrane, which facilitates the rapid migration of protons through the hydrogen bond network and enhances the proton conductivity of the membrane.

3.4 Proton conductivity

Proton conductivity (σ) is one of the most crucial parameters employed to evaluate the performance of PEMs in fuel cells [45]. A direct current (DC) conductivity test was performed to rule out any influence of electron conductivity on the performance of SPAEK and SPAEK-PW_{12} membranes (Fig. S8 in the ESM). The temperature-dependent proton conductivities of the pristine membrane and hybrid membranes with increasing amounts of PW_{12} were measured by alternating current impedance in water, as shown in Fig. 3(c). All the membranes exhibited a significant increase in proton conductivity as the temperature increased from 30 to 80 °C as a result of the thermal activation of proton transport. The pristine membrane exhibited proton conductivities of 0.037 S·cm^{-1} at 30 °C and 0.077 S·cm^{-1} at 80 °C in a water solution (Table S1 in the ESM). For comparison, the proton conductivity of the hybrid membrane increased notably as the content of PW_{12} increased. Notably, SPAEK-PW_{12}-13% exhibited the highest proton conductivity, ranging from 0.080 S·cm^{-1} at 30 °C to 0.167 S·cm^{-1} at 80 °C, which was better than those of most reported hybrid PEMs constructed on SPAEK (Table S2 in the ESM) [55, 56]. The proton conductivity of SPAEK-PW_{12}-13% was ~ 2.2 times higher than that of the pristine membrane at 30–80 °C. The main reasons for the above results are as follows. First, the hydrophilic PW_{12}, as a proton

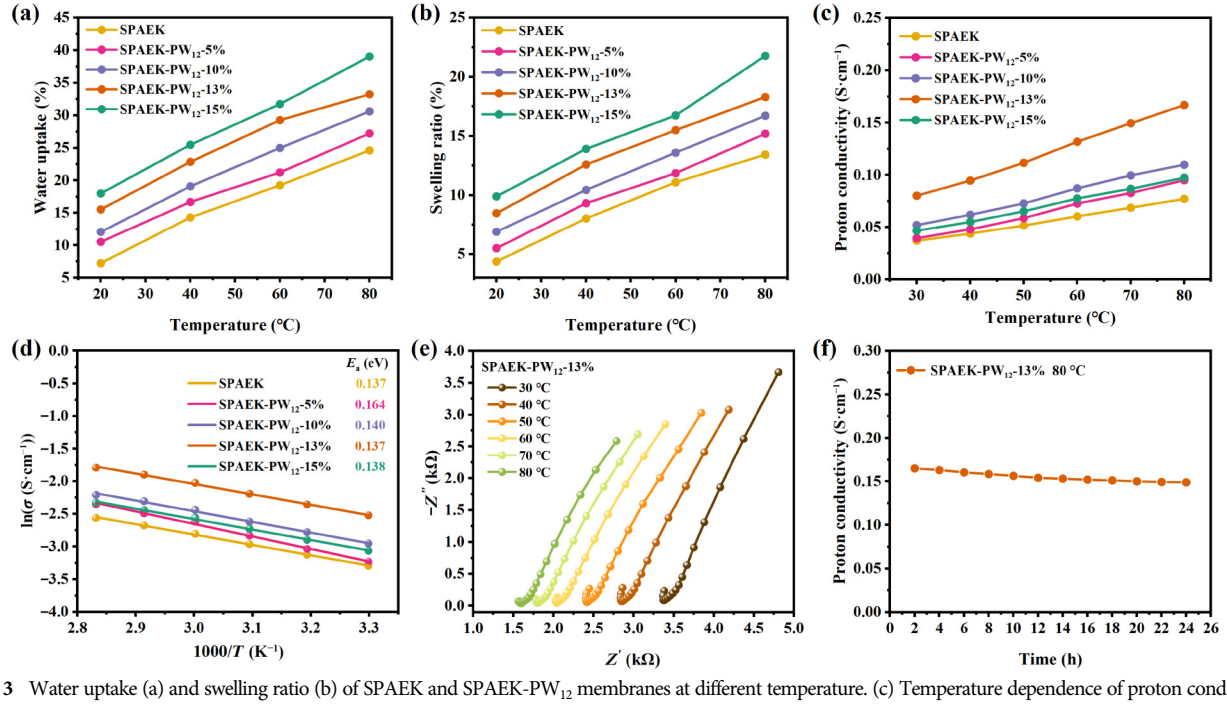

Figure 3 Water uptake (a) and swelling ratio (b) of SPAEK and SPAEK-PW_{12} membranes at different temperature. (c) Temperature dependence of proton conductivity of hybrid SPAEK-PW_{12} membranes in water solution. (d) Arrhenius-type plots of the conductivity of SPAEK and SPAEK-PW_{12} membranes at various temperatures and in water solution. (e) Nyquist plots of SPAEK-PW_{12}-13% membranes in water solution and various temperatures. (f) Proton conductivity of SPAEK-PW_{12}-13% membranes in water solution at 80 °C for last 24 h.

donor, increased the concentration of proton carriers and the amount of adsorbed water in the hybrid membrane, thus increasing the number of proton hopping sites. Second, the molecular-level hybridization of POMs extended the dimensions of the hydrophilic channels in the PEMs, as observed in TEM images, which in turn provided long-range continuous paths for proton transmission. Third, the strong hydrogen bonds between highly condensed ion clusters ($-SO_3H-H_2O$, $-SO_3H-PW_{12}$, and $-SO_3H-SO_3H$) in the hybrid membranes induced the formation of continuous proton transmission channels, which enhanced the transport of protons within the membranes. Protons could swiftly rotate and orient within the well-developed water-mediated hydrogen-bonding network, thereby facilitating rapid transfer.

Next, the activation energy of proton conduction for the membranes was calculated using the Arrhenius equation, $\sigma T = \sigma_0 \exp(-E_a/K_B T)$, to explore proton migration barriers [57]. As shown in Figs. 3(d) and 3(e)) and Fig. S9 in the ESM, the activation energies (E_a) for all membranes were approximately 0.13–0.16 eV in the temperature range of 30–80 °C in a water solution, corresponding to the Grotthuss-type mechanism [58]. Protons could rapidly rotate and reorient in the form of hydronium ions (H_3O^+, $H_5O_2^+$, and $H_9O_4^+$) in the water-filled channels of the hybrid membranes or migrate along the well-connected H-bond network formed by water molecules and proton-conductive groups ($-SO_3H$ and $-OH$) in the hybrid membranes. However, upon further addition of PW_{12}, SPAEK-PW_{12}-15% exhibited lower proton conductivity than SPAEK-PW_{12}-13%, which was attributed to the excessive accumulation of PW_{12} in the nanophases of the hybrid membrane, which disrupted the proton transport pathway. To evaluate the persistence of the proton conductivity of the SPAEK-PW_{12}-13% hybrid membrane, we measured the impedance of this membrane in deionized water at 80 °C continuously for 24 h (Fig. 3(f)). The proton conductivity of SPAEK-PW_{12}-13% remained basically constant at ~ 0.16 S·cm^{-1}, confirming the relatively long-term durability of this membrane under these operating conditions.

3.5 Mechanical properties and chemical stability

Mechanical properties are important parameters that affect the long-term stable operation of hybrid membranes [59]. As shown in Table 2, the tensile strength and elongation at break of the hybrid membranes with an appropriate content of PW_{12} ($x \leq 13$) were improved relative to those of the pristine membrane. SPAEK has satisfactory mechanical properties, with a tensile strength of 53.0 MPa and an elongation at break of 126.2%. Upon the addition of PW_{12}, the mechanical properties of SPAEK-PW_{12}-13% improved, resulting in a tensile strength of 65.1 MPa and an elongation at break of 154.8%. This occurred primarily because the strong hydrogen bonds between PW_{12} and $-SO_3H$ made the internal structure of the membrane more compact, as observed in the SEM images. Nevertheless, the mechanical properties of SPAEK-PW_{12}-15% decreased significantly because the excessive addition of PW_{12} may have caused aggregation of POM clusters that weakened the interfacial adhesion between the nanofillers and SPAEK.

Another parameter that affects the long-term stable operation of hybrid membranes is the oxidation stability of PEMs [60]. The membranes were soaked in a Fenton reagent to test the antioxidant stability, and the results are shown in Table 2. After being treated with the Fenton reagent at 80 °C, all the membranes experienced a certain weight loss. With the addition of PW_{12}, the weight retention rate of the hybrid membranes was improved. The fracture time of SPAEK-PW_{12}-13% was approximately 1.5 times longer than that of SPAEK because PW_{12} promoted decomposition of free radicals, thus preventing the hybrid membrane from being attacked by free radicals [61, 62].

3.6 Methanol permeability test

A methanol permeability (P) test was performed to evaluate the ability of SPAEK and the SPAEK-PW_{12}-x% (x = 5, 10, 13, 15) membranes to resist fuel penetration. The methanol permeability of SPAEK was 1.03 × 10^{-7} cm^{-2}·s^{-1} (Fig. 4). In addition, the PW_{12}-loaded hybrid membranes SPAEK-PW_{12}-x% exhibited a superior ability to prevent methanol crossover. This finding was attributed to the incorporation of PW_{12} in the ion channels of SPAEK, which resulted in a tortuous path for methanol and thus suppressed the permeability. Strong hydrogen-bonding between the hydrophilic PW_{12} and the sulfonic acid groups of SPAEK prevented methanol crossover. The methanol permeability of the SPAEK-PW_{12}-x% hybrid membranes decreased with increasing weight percent of the additive. For example, SPAEK-PW_{12}-13% exhibited a methanol permeability (P) of 3.95 × 10^{-8} cm^{-2}·s^{-1}. For SPAEK-PW_{12}-15%, the excessive introduction of PW_{12} destroyed the compact structure of the hybrid membrane and thus hindered the penetration of methanol.

Ionic selectivity suggests a balance between proton conductivity and methanol permeability. Figure 4 represents the ionic selectivity of SPAEK and various SPAEK-PW_{12}-x% (x = 5, 10, 13, 15) membranes. The ionic selectivity values of SPAEK and SPAEK-PW_{12}-13% were 3.65 × 10^5 and 2 × 10^6 S·s·cm^{-3}, respectively. The ionic selectivity of SPAEK-PW_{12}-13% was approximately one order of magnitude greater than that of SPAEK. Briefly, a certain amount of PW_{12} in the hybrid membrane formed a dense hydrogen-bonding network with the sulfonic acid groups in PEM to achieve an appropriate balance among various factors of the hybrid membrane.

4 Conclusions

In summary, we have developed a strategy to introduce PW_{12} into

Table 2 Crystallinity, mechanical properties and chemical stability of membranes

Samples	Tensile strength (MPa)	Elongation at break (%)	Young's modulus (GPa)	WR[a] (wt.%)	τ[b] (min)
SPAEK	53.0	126.2	1.10	92.9	300
SPAEK-PW_{12}-5%	57.3	142.1	0.72	94.8	390
SPAEK-PW_{12}-10%	61.6	140.6	0.66	95.4	408
SPAEK-PW_{12}-13%	65.1	154.8	0.56	98.4	432
SPAEK-PW_{12}-15%	52.4	85.4	0.44	98.5	438

[a]WR: the weight retention rate of the hybrid membrane after it began to break in Fenton's reagent (3% H_2O_2 and 2 ppm Fe^{2+}). [b]τ: the time when the membrane began to break in Fenton's reagent (3% H_2O_2 and 2 ppm Fe^{2+}).

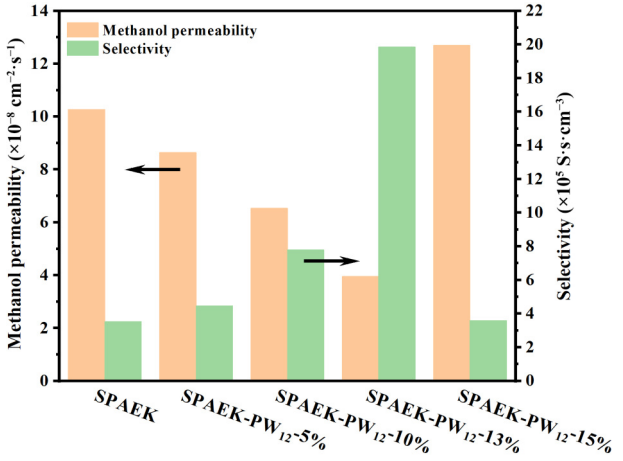

Figure 4 The methanol permeability and ionic selectivity of SPAEK-PW_{12}-*x*% (*x* = 0, 5, 10, 13, 15).

SPAEK and fabricated a series of hybrid membranes with comprehensive high performance. Sulfonated poly(arylene ether sulfone) with a high density of flexible side chains was successfully synthesized and used to make films that maintained a high proton conductivity and mechanical strength. Because of electrostatic forces, PW_{12} successfully entered into the ionic nanophase of membranes to form a stable microphase separation structure. Additionally, hydrogen-bonding networks were formed between PW_{12} and sulfonic acid groups, which increased the proton conductivity and mechanical strength and improved the close-packed structure of the resulting hybrid PEMs to achieve an appropriate balance between the conductivity and fuel permeation. Specifically, the SPAEK-PW_{12}-13% hybrid membrane exhibited a proton conductivity of 0.167 S·cm^{-1} at 80 °C in a water solution, which was 220% times greater than that of the pristine SPAEK under the same conditions. In addition, the SPAEK-PW_{12}-13% hybrid membrane exhibited satisfactory mechanical and chemical stability, relatively low methanol permeability, and high ionic selectivity. This work demonstrates the advantages of POMs as inorganic proton conductors comprehensively improve the performance of polymer-based hybrid PEMs, which can lead to the development of a new generation of high-performance materials and energy devices.

Electronic Supplementary Material: Supplementary material (PXRD, IR, Raman, TG, and proton conductivities of all compounds and corresponding Nafion composite Membranes) is available in the online version of this article at https://doi.org/10.26599/POM.2024.9140079.

Data availability

All data needed to support the conclusions in the paper are presented in the manuscript and the Electronic Supplementary Material. Additional data related to this paper may be requested from the corresponding author upon request.

Acknowledgements

The authors gratefully acknowledge the financial support from the Natural Science Foundation of Jilin Province (No. 20210101132JC), the Natural Science Foundation of Chongqing City (No. cstc2021jcyj-msxmX1209), and the National Natural Science Foundation of China (Nos. 22101031 and 22322102). We acknowledge the support from the Northeast Normal University, Key Laboratory of Polyoxometalate and Reticular Material Chemistry of the Ministry of Education, Fundamental Research Funds for the Central Universities (No. 2412023QD011), and the Jilin Provincial Department of Education (Nos. JJKH20240902KJ and JJKH20210805KJ).

Declaration of competing interest

The authors have no competing interests to declare that are relevant to the content of this article. Author Yangguang Li is the associate editor of this journal and author Zhongmin Su is the advisory board member of this journal, but them are not involved in the peer-review or decision of this article.

Author contribution statement

B. H.: Data curation, formal analysis, writing manuscript, experimental design. Q. C. D. and Y. Y.: Synthesis, data curation, formal analysis. D. D. L. and J. W. F.: Validation. B. L. L., H.-Y. Z. and Y. G. L.: Project administration, funding acquisition, writing-reviewing and editing manuscript. H. M. X. and Z. M. S.: Supervision, reviewing. All the authors have approved the final manuscript.

Use of AI statement

None.

References

[1] Li, J. B.; Cui, N.; Liu, D.; Zhao, Z.; Yang, F.; Zhong, J. D.; Pang, J. H. SPEEK-co-PEK-x proton exchange membranes with controllable sulfonation degree for proton exchange membrane fuel cells. *Int. J. Hydrogen Energy* **2024**, *50*, 606–617.

[2] Zhu, S. H.; Zhang, Y. Y.; Zhang, J.; Ma, J. Y.; Li, S. H.; Dai, P.; Wu, Y. X. High-performance proton exchange membrane of sulfonated polystyrene-*b*-polyisobutylene-*b*-polystyrene. *ACS Appl. Polym. Mater.* **2024**, *6*, 3930–3941.

[3] Gittleman, C. S.; Jia, H. F.; De Castro, E. S.; Chisholm, C. R. I.; Kim, Y. S. Proton conductors for heavy-duty vehicle fuel cells. *Joule* **2021**, *5*, 1660–1677.

[4] Guan, J. Y.; Sun, X.; Yu, H. T.; Zheng, J. F.; Sun, Y. X.; Li, S. H.; Qin, G. R.; Zhang, S. B. High conductive and dimensional stability proton exchange membranes with an all-carbon main chain and densely sulfonated structure. *J. Membr. Sci.* **2024**, *700*, 122664.

[5] Bai, X. T.; Cao, L. H.; Ji, C.; Zhao, F.; Chen, X. Y.; Cao, X. J.; Huang, M. F. Ultra-high proton conductivity iHOF based on guanidinium arylphosphonate for proton exchange membrane fuel cells. *Chem. Mater.* **2023**, *35*, 3172–3180.

[6] Chao, G.; Zhang, Z. G.; Lv, Z. X.; Yang, E. Q.; Gao, R. F.; Ju, Q.; Gao, H.; Niu, C. Y.; Qian, H. D.; Geng, K. et al. Copolymerized sulfonated poly(oxindole biphenylene) polymer electrolyte for proton exchange membrane fuel cells. *J. Membr. Sci.* **2024**, *700*, 122674.

[7] Katzenberg, A.; Chowdhury, A.; Fang, M. F.; Weber, A. Z.; Okamoto, Y.; Kusoglu, A.; Modestino, M. A. Highly permeable perfluorinated sulfonic acid ionomers for improved electrochemical devices: Insights into structure-property relationships. *J. Am. Chem. Soc.* **2020**, *142*, 3742–3752.

[8] Zuo, P. P.; Li, Y. Y.; Wang, A. Q.; Tan, R.; Liu, Y. H.; Liang, X.; Sheng, F. M.; Tang, G. G.; Ge, L.; Wu, L. et al. Sulfonated microporous polymer membranes with fast and selective ion transport for electrochemical energy conversion and storage. *Angew. Chem.,*

Int. Ed. **2020**, *59*, 9564–9573.
[9] Ji, J. Y.; Han, Y. Y.; Xu, F.; Chu, F. Q.; Li, Y. T.; Lin, B. C. Guanidinium/hydroxyl-functionalized polybenzimidazole for high-temperature proton exchange membrane fuel cell applications. *ACS Appl. Energy Mater.* **2023**, *6*, 11754–11761.
[10] Li, T. T.; Chai, S. C.; Liu, B. H.; Zhao, C. J.; Li, H. L. All-carbon backbone aromatic polymers for proton exchange membranes. *J. Polym. Sci.* **2023**, *61*, 2796–2814.
[11] Wang, Y.; Wang, Y. M.; Wang, Y. Z.; Su, B. H.; Shi, L. L.; Li, F. B.; Mu, J. B.; Che, H. W.; Zhang, Z. X.; Zhang, X. L. et al. Preparation and performance study of ionic liquid @ boron nitride modified polyimide proton exchange membrane. *Polym. Compos.* **2023**, *44*, 5527–5538.
[12] Shao, Z. C.; Xue, X. J.; Gao, K. X.; Chen, J. S.; Zhai, L. P.; Wen, T. Y.; Xiong, S. L.; Hou, H. W.; Mi, L. W. Sulfonated covalent organic framework packed Nafion membrane with high proton conductivity for H_2/O_2 fuel cell applications. *J. Mater. Chem. A* **2023**, *11*, 3446–3453.
[13] Zhao, S. Q.; Liao, Y. C.; Wang, R.; Liu, G. L.; Zhang, H. N.; Tang, H. L. Polyphenol synergistic cerium oxide surface engineering constructed core-shell nanostructures as antioxidants for durable and high-performance proton exchange membrane fuel cells. *Chem. Eng. J.* **2023**, *472*, 144804.
[14] Poongan, A.; Kesava, M.; Mandal, A.; Murugan, E. Effect of ZrO_2 nanoparticles on phosphoric acid-doped poly(ethylene imine)/polyvinyl alcohol) membrane for medium-temperature polymer electrolyte membrane fuel cell applications. *Int. J. Hydrogen Energy* **2023**, *48*, 27371–27382.
[15] Liu, Q. T.; Ling, Z. W.; Wang, X. H.; Fu, X. D.; Wu, W. Z.; Xiong, C. Y.; Wang, B.; Zhang, R.; Li, X.; Zhao, F. et al. Polyethyleneimine-confined halloysite nanotubes for poly(2,5-benzimidazole) composite membranes with phosphoric acid retention and proton conductivity via ion pairs for wide-temperature PEMFCs. *Compos. Sci. Technol.* **2023**, *242*, 110199.
[16] Liu, K.; Wei, X. Q.; Hu, S.; Li, Q. Q.; Gao, W. M.; Wu, D.; Che, Q. T. Enhancing proton conduction of high temperature proton exchange membranes based on carbon dots doped polyvinyl chloride nanofibers. *Sep. Purif. Technol.* **2023**, *325*, 124679.
[17] Zhai, S. X.; Lu, Z. R.; Ai, Y. N.; Jia, X. Y.; Yang, Y. M.; Liu, X.; Tian, M.; Bian, X. M.; Lin, J.; He, S. J. High performance nanocomposite proton exchange membranes based on the nanohybrids formed by chemically bonding phosphotungstic acid with covalent organic frameworks. *J. Power Sources* **2023**, *554*, 232332.
[18] Maegawa, K.; Nagai, H.; Kumar, R.; Abdel-Galeil, M. M.; Tan, W. K.; Matsuda, A. Development of polybenzimidazole modification with open-edges/porous-reduced graphene oxide composite membranes for excellent stability and improved PEM fuel cell performance. *Mater. Chem. Phys.* **2023**, *294*, 126994.
[19] Wei, P.; Sui, Y.; Zhu, B. S.; Meng, X. Y.; Zhou, Q. Construction of continuous proton transport channels in SPEEK using porous titanium dioxide nanotubes. *Solid State Ionics* **2023**, *399*, 116321.
[20] Chen, X.; Ren, Q.; Xu, J. M.; Ju, M. C.; Meng, L. X.; Wang, Z. Design, transport efficiency and structure-activity relationship of sulfonated poly (aryl ether ketone) proton exchange membrane based on multi-functional MOFs. *Electrochim. Acta* **2023**, *469*, 143210.
[21] Aziz, A.; Shanmugam, S. Ultra-high proton/vanadium selectivity of a modified sulfonated poly(arylene ether ketone) composite membrane for all vanadium redox flow batteries. *J. Mater. Chem. A* **2017**, *5*, 16663–16671.
[22] Chaturvedi, P.; Moehring, N. K.; Knight, T.; Shah, R.; Vlassiouk, I.; Kidambi, P. R. The parameter space for scalable integration of atomically thin graphene with Nafion for proton exchange membrane (PEM) applications. *Mater. Adv.* **2023**, *4*, 3473–3481.
[23] Yin, C. S.; Xiong, B. Y.; Liu, Q. C.; Li, J. J.; Qian, L. B.; Zhou, Y. W.; He, C. Q. Lateral-aligned sulfonated carbon-nanotubes/Nafion composite membranes with high proton conductivity and improved mechanical properties. *J. Membr. Sci.* **2019**, *591*, 117356.
[24] Ogiwara, N.; Iwano, T.; Ito, T.; Uchida, S. Proton conduction in ionic crystals based on polyoxometalates. *Coord. Chem. Rev.* **2022**, *462*, 214524.
[25] Zhai, L.; Zhu, Y. L.; Wang, G.; He, H. B.; Wang, F. R.; Jiang, F. J.; Chai, S. C.; Li, X.; Guo, H. K.; Wu, L. X. et al. Ionic-nanophase hybridization of nafion by supramolecular patching for enhanced proton selectivity in redox flow batteries. *Nano Lett.* **2023**, *23*, 3887–3896.
[26] Liu, M. L.; Han, X.; He, W. W.; Jiang, F. Y.; Ji, F.; Shen, W. W.; Zhou, T.; Xu, J. M.; Lan, Y. Q. Sulfonated poly (aryl ether ketone sulfone) modified by polyoxometalates LaW_{10} clusters for proton exchange membranes with high proton conduction performance. *Tungsten* **2024**, *6*, 454–464.
[27] Wang, G.; Li, J. L.; Zhai, L.; Li, X.; He, H. B.; Guo, H. K.; Li, H. B.; Zhao, C. J.; Wu, L. X.; Li, H. L. Polyoxometalate-polymer nanocomposites with multiplex proton transport channels for high-performance proton exchange membranes. *Compos. Sci. Technol.* **2023**, *232*, 109842.
[28] Glibin, V.; Vajihinejad, V.; Pupkevich, V.; Karamanev, D. G. Tailor-made phosphorylated polyvinyl alcohol/tungsten polyoxometalate proton exchange membrane for a bio-electrochemical energy storage system. *Energies* **2021**, *14*, 7975.
[29] Zeng, M. H.; Liu, W. Q.; Guo, H. K.; Li, T. T.; Li, Q. J.; Zhao, C. J.; Li, X. J.; Li, H. L. Polyoxometalate-cross-linked proton exchange membranes with post-assembled nanostructures for high-temperature proton conduction. *ACS Appl. Energy Mater.* **2022**, *5*, 9058–9069.
[30] Kondinski, A. Superchaotropic polyoxometalates as membrane carriers. *Polyoxometalates* **2024**, *3*, 9140058.
[31] Liu, Q. Q.; Cui, Y. Z.; Zhu, L. J.; Cheng, D. M.; Wang, C.; Lu, S. Q.; Li, B.; Chen, X. Y.; Zang, H. Y. Ionic liquid-mediated PEO-based solid-state electrolyte membrane modified with Dawson-type polyoxometalates. *Polyoxometalates* **2023**, *2*, 9140036.
[32] Zhai, L.; Li, H. L. Polyoxometalate-polymer hybrid materials as proton exchange membranes for fuel cell applications. *Molecules* **2019**, *24*, 3425.
[33] Cheng, D. M.; Li, K.; Zang, H. Y.; Chen, J. J. Recent advances on polyoxometalate-based ion-conducting electrolytes for energy-related devices. *Energy Environ. Mater.* **2023**, *6*, e12341.
[34] Liu, W. J.; Dong, L. Z.; Li, R. H.; Chen, Y. J.; Sun, S. N.; Li, S. L.; Lan, Y. Q. Different protonic species affecting proton conductivity in hollow spherelike polyoxometalates. *ACS Appl. Mater. Interfaces* **2019**, *11*, 7030–7036.
[35] Li, S. J.; Zhao, Y.; Knoll, S.; Liu, R. J.; Li, G.; Peng, Q. P.; Qiu, P. T.; He, D. F.; Streb, C.; Chen, X. N. High proton-conductivity in covalently linked polyoxometalate-organoboronic acid-polymers. *Angew. Chem., Int. Ed.* **2021**, *60*, 16953–16957.
[36] Hu, Q. L.; Li, K.; Chen, X. J.; Liu, Y. F.; Yang, G. P. Polyoxometalate catalysts for the synthesis of N-heterocycles. *Polyoxometalates* **2024**, *3*, 9140048.
[37] Wang, P.; Wang, Z. T.; Wang, P. S.; Chishti, A. N.; Zhang, H. X.; Shi, J. H.; Ni, L. B.; Jamil, S.; Wei, Y. G. Supramolecular self-assembly of polyoxometalates and cyclodextrin: Progress and perspectives. *Polyoxometalates* **2024**, *3*, 9140047.
[38] Zhang, H. Y.; Zhao, W. L.; Li, H. Q.; Zhuang, Q. H.; Sun, Z. Q.; Cui, D. Y.; Chen, X. J.; Guo, A.; Ji, X.; An, S. et al. Latest progress in covalently modified polyoxometalates-based molecular assemblies and advanced materials. *Polyoxometalates* **2022**, *1*, 9140011.
[39] Liu, Y. F.; Lin, X. L.; Ming, B. M.; Hu, Q. L.; Liu, H. Q.; Chen, X. J.; Liu, Y. H.; Yang, G. P. Three polyoxometalate-based Ag-organic compounds as heterogeneous catalysts for the synthesis of benzimidazoles. *Inorg. Chem.* **2024**, *63*, 5681–5688.
[40] Wang, Y. D.; Wang, J. X.; Wei, M. J.; Liu, B. L.; Zang, H. Y.; Tan, H. Q.; Wang, Y. H.; Li, Y. G. Niobium oxyhydroxide-polyoxometalate composite as an efficient proton-conducting solid electrolyte. *ChemElectroChem* **2018**, *5*, 1125–1129.

[41] Liu, W. D.; Zhu, H. T.; Zhang, X.; Su, F.; Sang, X. J.; Zhang, X. L.; Zhang, L. C. Room temperature self-assembly and nonenzymatic electrochemical sensing performance of transition metal-embedded wheel-shaped tungstophosphates. *Polyoxometalates* **2025**, *4*, 9140073.
[42] Niinomi, K.; Miyazawa, S.; Hibino, M.; Mizuno, N.; Uchida, S. High proton conduction in crystalline composites based on preyssler-type polyoxometalates and polymers under nonhumidified or humidified conditions. *Inorg. Chem.* **2017**, *56*, 15187–15193.
[43] Li, X. X.; Li, C. H.; Hou, M. J.; Zhu, B.; Chen, W. C.; Sun, C. Y.; Yuan, Y.; Guan, W.; Qin, C.; Shao, K. Z. et al. Ce-mediated molecular tailoring on gigantic polyoxometalate $\{Mo_{132}\}$ into half-closed $\{Ce_{11}Mo_{96}\}$ for high proton conduction. *Nat. Commun.* **2023**, *14*, 5025.
[44] Wang, Y. X.; Lu, Y.; Zhang, W. S.; Dang, T. Y.; Yang, Y. L.; Bai, X.; Liu, S. X. Construction of hydrogel composites with superior proton conduction and flexibility using a new POM-based inorganic-organic hybrid. *Polyoxometalates* **2022**, *1*, 9140005.
[45] Liu, B. L.; Hu, B.; Du, J.; Cheng, D. M.; Zang, H. Y.; Ge, X.; Tan, H. Q.; Wang, Y. H.; Duan, X. Z.; Jin, Z. et al. Precise molecular-level modification of nafion with bismuth oxide clusters for high-performance proton-exchange membranes. *Angew. Chem., Int. Ed.* **2021**, *60*, 6076–6085.
[46] He, H. B.; Zhu, Y. L.; Li, T. T.; Song, S. H.; Zhai, L.; Li, X.; Wu, L. X.; Li, H. L. Supramolecular anchoring of polyoxometalate amphiphiles into nafion nanophases for enhanced proton conduction. *ACS Nano* **2022**, *16*, 19240–19252.
[47] Ji, F.; Jiang, F. Y.; Luo, H. W.; He, W. W.; Han, X.; Shen, W. W.; Liu, M. L.; Zhou, T.; Xu, J. M.; Wang, Z. et al. Hybrid membrane of sulfonated poly(aryl ether ketone sulfone) modified by molybdenum clusters with enhanced proton conductivity. *Small* **2024**, *20*, 2312209.
[48] Wang, C. Y.; Li, N. W.; Shin, D. W.; Lee, S. Y.; Kang, N. R.; Lee, Y. M.; Guiver, M. D. Fluorene-based poly(arylene ether sulfone)s containing clustered flexible pendant sulfonic acids as proton exchange membranes. *Macromolecules* **2011**, *44*, 7296–7306.
[49] Liu, Y. F.; Zeng, G. D.; Cheng, Y. T.; Chen, L.; Liu, Y. H.; Wei, Y. G.; Yang, G. P. A $H_4SiW_{12}O_{40}$-catalyzed three-component tandem reaction for the synthesis of 3, 3-disubstituted isoindolinones. *Chin. Chem. Lett.* **2024**, *35*, 108480.
[50] Hu, B.; Liu, L. D.; Zhao, Y. X.; Lü, C. L. A facile construction of quaternized polymer brush-grafted graphene modified polysulfone based composite anion exchange membranes with enhanced performance. *RSC Adv.* **2016**, *6*, 51057–51067.
[51] He, H. B.; Song, S. H.; Zhai, L.; Li, Z. X.; Wang, S. H.; Zuo, P.; Zhu, Y. L.; Li, H. L. Supramolecular modifying nafion with fluoroalkyl-functionalized polyoxometalate nanoclusters for high-selective proton conduction. *Angew. Chem., Int. Ed.* **2024**, *63*, e202409006.
[52] Gahlot, S.; Sharma, P. P.; Kulshrestha, V.; Jha, P. K. SGO/SPES-based highly conducting polymer electrolyte membranes for fuel cell application. *ACS Appl. Mater. Interfaces* **2014**, *6*, 5595–5601.
[53] Neelakandan, S.; Jacob, K. N.; Kanagaraj, P.; Sabarathinam, R. M.; Muthumeenal, A.; Nagendran, A. Effect of sulfonated graphene oxide on the performance enhancement of acid-base composite membranes for direct methanol fuel cells. *RSC Adv.* **2016**, *6*, 51599–51608.
[54] Sweety, M. N.; Salam, A. Proton conductivity performance and its correlation with physio-chemical properties of proton exchange membrane (PEM). *Chin. J. Chem. Eng.* **2024**, *74*, 100–116.
[55] Xu, M. H.; Xue, H.; Wang, Q. F.; Jia, L. C. Sulfonated poly(arylene ether)s based proton exchange membranes for fuel cells. *Int. J. Hydrogen Energy* **2021**, *46*, 31727–31753.
[56] Maiti, T. K.; Singh, J.; Dixit, P.; Majhi, J.; Bhushan, S.; Bandyopadhyay, A.; Chattopadhyay, S. Advances in perfluorosulfonic acid-based proton exchange membranes for fuel cell applications: A review. *Chem. Eng. J. Adv.* **2022**, *12*, 100372.
[57] Wang, S. J.; Wahiduzzaman, M.; Davis, L.; Tissot, A.; Shepard, W.; Marrot, J.; Martineau-Corcos, C.; Hamdane, D.; Maurin, G.; Devautour-Vinot, S. et al. A robust zirconium amino acid metal-organic framework for proton conduction. *Nat. Commun.* **2018**, *9*, 4937.
[58] Li, Y. X.; Liang, L.; Liu, C. P.; Li, Y.; Xing, W.; Sun, J. Q. Self-healing proton-exchange membranes composed of nafion-poly(vinyl alcohol) complexes for durable direct methanol fuel cells. *Adv. Mater.* **2018**, *30*, 1707146.
[59] Shigematsu, A.; Yamada, T.; Kitagawa, H. Wide control of proton conductivity in porous coordination polymers. *J. Am. Chem. Soc.* **2011**, *133*, 2034–2036.
[60] Shen, X. H.; Liang, X.; Xu, Y.; Yu, W. S.; Li, Q. H.; Ge, X. L.; Wu, L.; Xu, T. W. *In-situ* growth of PPy/MnO_x radical quenching layer for durability enhancement of proton exchange membrane in PEMFCs. *J. Membr. Sci.* **2023**, *675*, 121556.
[61] Bokare, A. D.; Choi, W. Review of iron-free Fenton-like systems for activating H_2O_2 in advanced oxidation processes. *J. Hazard. Mater.* **2014**, *275*, 121–135.
[62] Lei, S.; Yang, H.; Li, J. X.; Li, Y.; Wang, L.; Chen, B. N.; Li, J. A study of the antioxidant properties of Keggin-type polyoxometalates. *Dalton Trans.* **2023**, *52*, 9673–9683.

Bo Hu received his Ph.D. degree from Northeast Normal University. He is currently a lecturer in the Faculty of Chemistry, Northeast Normal University. He is mainly engaged in the preparation and modification of polyethersulfone modified proton and anion exchange membrane, and the research of polymer-based solid electrolyte.

Qiuchen Du received his B.S. degree in chemistry from Shangqiu Normal University in 2022. He is currently studying for a master's degree in Changchun University of Science and Technology. His research focuses on polyoxometalates hybrid modified high-temperature proton exchange membranes.

Bailing Liu received her Ph.D. degree from Northeast Normal University. She is currently an associate professor and master supervisor at the School of Chemical and Environmental Engineering, Changchun University of Science and Technology. She is mainly engaged in the synthesis of polyoxometalates-supported two-dimensional layered materials and polyoxometalates-modified polymer proton exchange membranes, as well as research in the field of proton conductors and fuel cells.

Hong-Ying Zang is a professor and doctoral supervisor at Northeast Normal University. She obtained a master's degree in 2007–2010 under the tutelage of Professor Zhongmin Su, and received her Ph.D. from the University of Glasgow under the tutelage of Professor Leroy Cronin and conducted post-doctoral research in 2010–2014. She established an independent research group in 2014. Her research work mainly focuses on the synthesis and assembly of polymetallic oxygen clusters and their basic application research in energy conversion and storage, including the ion conductivity of cluster-based solid materials, the role of polymetallic oxygen cluster materials in energy conversion.

Yangguang Li is a professor at the Faculty of Chemistry at Northeast Normal University. He conducts research in polyoxometalate chemistry, combining fundamental research on polyoxometalates with sustainable hydrogen production. He has carried out systematic research work in the areas of directed synthesis of polyoxometalates, design and preparation of catalytic materials, and electrolysis of water to produce hydrogen.